

# Educational Experimental Rig for Doubly-Fed Induction Generator based Wind Turbine

M. Suwan, T. Neumann, C. Feltes, *Member, IEEE*, and I. Erlich, *Senior Member, IEEE*

**Abstract**—An experimental rig for grid-connected Doubly-Fed Induction Generator (DFIG) based wind turbine is presented. The experimental rig was developed for educational and research purposes at the University Duisburg Essen. The goal here is to give an overview of the structure, control and operation of the developed DFIG system. Independent control of active and reactive power of the generator is achieved by applying voltage-oriented control schemes. In the laboratory set up, a 9kW slip ring induction generator is used. The generator is driven by a torque-controlled squirrel cage induction motor. The control program of the wind turbine emulator generates the torque reference value for the drive. The commissioning procedure through the PC user interface is described. The performance of the developed rig is demonstrated through experimental results during nominal load operation.

**Index Terms**—wind power, doubly-fed induction generator, line side converter, machine side converter, emulator.

## I. NOMENCLATURE

$\underline{i}_S, \underline{i}_R$	Complex stator and rotor currents
$\underline{v}_S, \underline{v}_R$	Complex stator and rotor terminal voltages
$\underline{v}_{LSC}, \underline{i}_{LSC}$	Complex LSC voltage and current
$\underline{v}_{DC}, \underline{i}_{DC}$	Converter DC-link voltage and current
$\underline{\psi}_S, \underline{\psi}_R$	Complex stator and rotor flux-linkages
$l_{\sigma S}, l_{\sigma R}$	Stator and rotor leakage inductances (per unit), they correspond with the reactances $x_{\sigma S}, x_{\sigma R}$
$l_h$	Main-field inductance (per unit), it corresponds with the reactance $x_h$
$r_S, r_R$	Stator and rotor resistances
$\omega_R, \omega_0$	Rotor angular speed, synchronous speed
$v_w$	Wind speed
$\beta$	Pitch angle
$t_{el}, t_m$	Electrical/mechanical torque
<u>Superscripts/Subscripts</u>	
d, q	Direct, quadrature axis component
$\angle^*$	Reference frame, $\angle$ : arbitrary, $\angle v_g$ : grid voltage oriented,
$\angle v_S$	stator voltage oriented

M. Suwan, T. Neumann and I. Erlich are with the Institute of Electrical Power Systems, University Duisburg Essen, Bismarckstr. 81, 47057 Duisburg, Germany (e-mails: mohammad.suwan@uni-due.de; tobias.neumann@uni-due.de; istvan.erlich@uni-due.de).

C. Feltes is with RWE Innogy, Hamburg, Germany (e-mail: christen.feltes@rwe.com).

## II. INTRODUCTION

IN the recent years renewable energy sector enjoyed worldwide a rapid capacity growth. Being by far the most promising and technically advanced renewable power source, wind energy generation related projects and studies have scaled up significantly. Therefore there is a growing academic interest in practically demonstrating technologies of wind power conversion systems. One of these technologies is the DFIG. Compared to the full rated converter system, the DFIG is still having appreciable economic advantages in several applications.

Various papers dealt with developing DFIG experimental systems as early as [1]. However most of the papers did not highlight the educational competencies in developing such a system. This paper offers an overall description of the developed experimental rig with its adequate user interface programmed in a graphical simulation environment.

The main motivations behind this work are to demonstrate the control and operation concept of the DFIG and to conduct tests for power system stability studies by applying simulated grid faults. The DFIG system was developed in stages throughout students undergraduate and graduate projects. Presently, the experimental rig is used in the lab for education and research purposes, and undergoes continuous improvements through student projects.

The basic concept of the DFIG is described briefly in the next section. Section IV offers an overview of hardware and software components of the developed rig. The main control concepts of the DFIG are discussed in section V. In section VI, the emulation concept is presented based on a modern strategy for wind turbine control. The paper ends with the demonstration the PC user interface with test results and concluding remarks.

## III. DFIG TECHNOLOGY

Fig. 1 shows the basic concept of a wind turbine based on DFIG technology. The mechanical torque generated at the wind turbine shaft drives the DFIG. As the generator rotates mechanical power will be converted into electrical power through its rotor and stator windings feeding the connected grid. The DFIG system ensures efficient power conversion due to variable rotor speed. According to the prevailing wind speeds, the rotor speed is adjusted (or limited) using speed and pitch control. Basically the control of the DFIG can be separated into the line side converter (LSC) and the machine

side converter (MSC) controls. The functions and control concepts of both converters are described in section V.

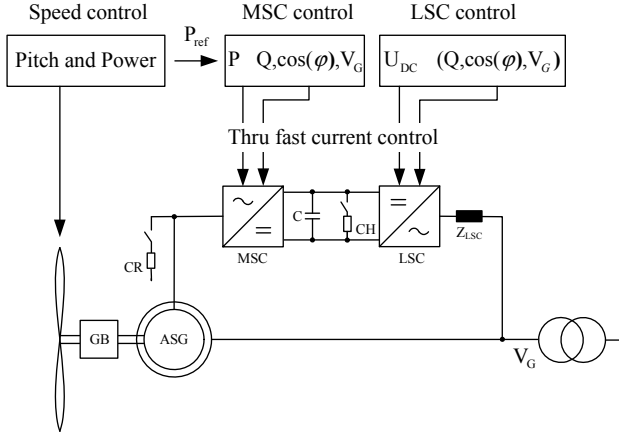


Fig. 1. Basic concept DFIG- based wind turbine system

Variable speed operation of the DFIG is made possible by directionally dependent transfer of slip power via the frequency converter [2]. Thus two operation modes are possible; subsynchronous and supersynchronous operation modes. In the subsynchronous mode (partial load range), the stator of the DFIG supplies power to the grid and also the slip power to the rotor via slip rings and the converters. While in the supersynchronous mode (nominal load range), both the stator output power and the rotor slip power are fed to the grid. Usually the nominal generator speed is specified well above the synchronous speed (supersynchronous mode) in order to operate with maximum efficiency; this speed point corresponds to the rated wind velocity. By choosing a higher speed operation point, more power will be transferred through the rotor. Due to the voltage limit of the converters, the operation speed is limited to a certain range. Therefore at full load, the active power passing through the rotor circuit amounts to roughly 17% of total power, while the speed range is  $\pm 33\%$  around the synchronous speed.

#### IV. EXPERIMENTAL RIG STRUCTURE

##### A. Hardware Components

Fig. 2 shows the three-phase circuit diagram of the experimental rig. Basically [3] the rig setup can be separated into five parts: a) Drive train, b) transformer, c) power electronics, d) Digital Signal Processor (DSP) and e) Fault Ride Through (FRT) testing set up.

In this experimental rig, a 50Hz, 11kW, 400V, 2-pole pair slip ring induction generator is driven by a standard squirrel cage asynchronous motor emulating the wind turbine prime mover (Fig. 3). The driving motor is controlled by a commercial variable-frequency converter; the emulation concept is discussed in section VI. The voltage level of the DFIG is limited to 200V due to the saturation effects in the generator. Thus the whole DFIG system has a rated power of 9 kW including the LSC.

A Dyn5 transformer is connected to the low voltage level through its primary winding, while the voltage level of the secondary winding can be adjusted. During grid side faults,

the  $\Delta$ -Y connection of the transformer decouples the zero sequence system. Therefore only positive and negative sequence quantities will remain on the generation unit side.

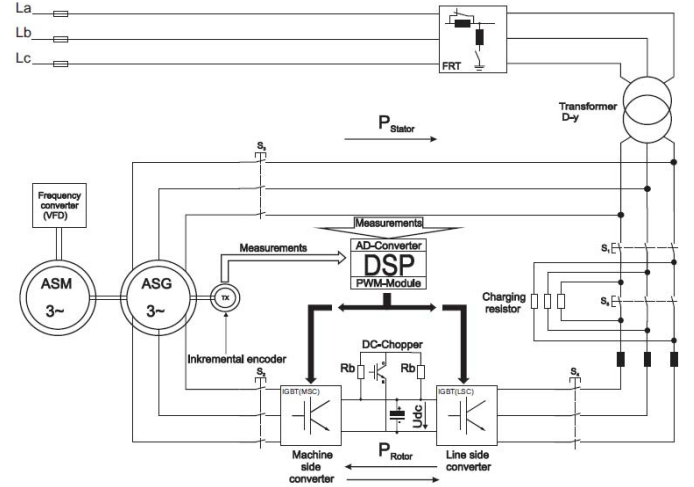


Fig. 2. Circuit diagram of the experimental rig

In the state of the art wind turbines as well as in the experimental rig 2-level IGBT converters are used. These back-to-back PWM voltage-source converters were assembled at the university laboratory. The functions of these converters are a) converting AC to DC and back to AC at variable frequency, b) controlling DC-link voltage level and c) controlling amplitude, frequency and phase angle of rotor voltage. The switching frequency of the IGBT's (here 5 kHz) should be chosen in a way that the balance between switching losses and accuracy of the desired signals is achieved.

The DSP is one of the core elements of the experimental rig because it contains the control and thus the technical know-how. The DSP sends the PWM signals to each IGBT.

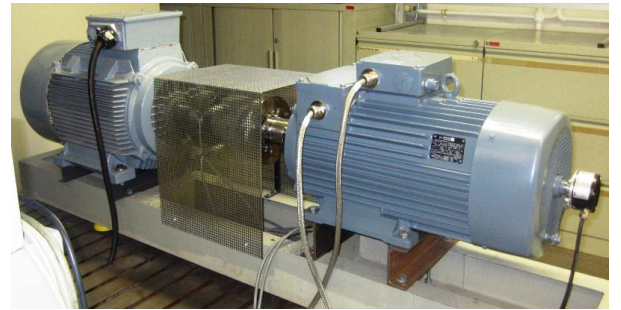


Fig. 3. Drive train of the experimental rig

An inductive voltage divider is used to produce voltage dips with defined depths and durations, and the FRT capability of the DFIG can be tested to determine whether it meets certain grid code requirements. Fig. 4 describes the basic set up for FRT testing.

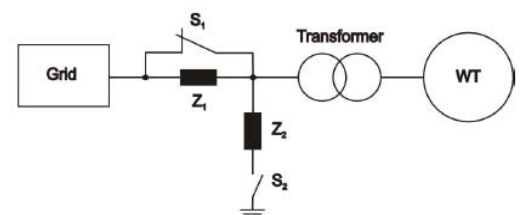


Fig. 4. Basic set-up for FRT testing set up

## B. Software Components

The programming of the DSP is done using MATLAB/Simulink, where the program is translated in C-code using the Automatic Code Generation tool integrated in MATLAB. The code is then transformed further into Assembly language level and finally to binary code that is sent to the DSP. This programming approach of the DSP and its benefits are discussed in details in [3].

Fig. 5 illustrates the main interfaces and data flow of the experimental rig. First, voltages and currents required for the control of the system are measured. Through transducers and signal conditioners the measured data are parameterized and processed so that it can be digitalized by the analog to digital converter (ADC) in the DSP as well as the Data Acquisition (DAQ) device. The received data in the DSP are further processed and control signals of the output variables are generated and modulated using the PWM technique. These PWM signals are the control signals of the IGBT's of both LSC and MSC.

For visualizing different measurements, adjusting setpoints and operation modes of the experimental rig the software LabVIEW is used. LabVIEW is a G-code based programming environment which offers a distinctive user interface through its "Front Panel". LabVIEW is commonly used for data acquisition, signal processing and visualization applications [4].

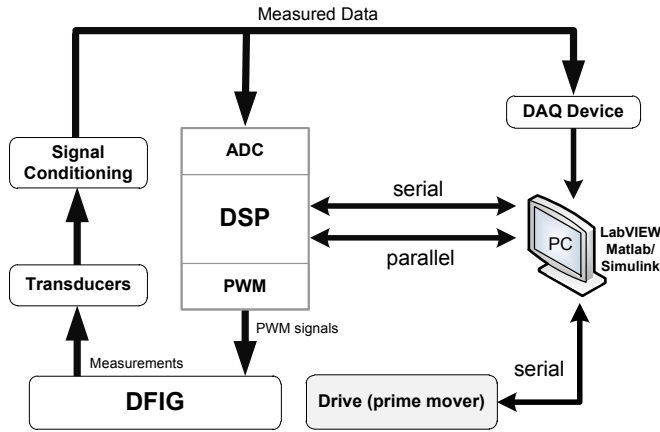


Fig. 5. Experimental rig interfaces and data flow

## V. THEORETICAL BACKGROUND AND BASIC CONTROL SCHEMES

### A. LSC Control

The function of the Line Side IGBT-Converter is to maintain the DC-link voltage level constant and to provide reactive current support for the optimization of the reactive power sharing between MSC and LSC in steady-state. According to certain grid codes, reactive power has to be supplied by the DFIG during short time grid faults in order to support the grid voltage. Fig. 6 shows the circuit diagram of the LSC, where  $v_g$  is the grid side voltage,  $i_{LSC}$  is the current between the grid and the IGBT Converter,  $C$  is the DC-link capacitor and  $L$  is the line inductance. In this paper, per unit

system is used.

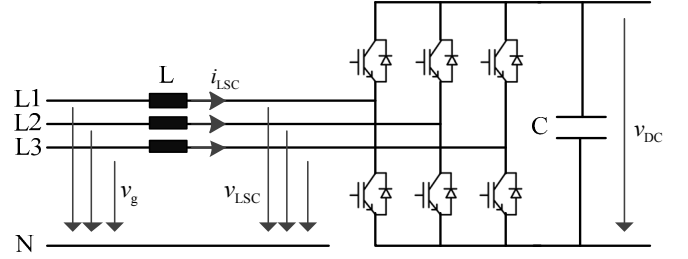


Fig. 6. LSC circuit diagram

Using the mesh analysis (starting from the grid voltage side through the voltage drop over the line inductances to the converter voltage side) we obtain (1).

$$\begin{pmatrix} v_{g,L1} \\ v_{g,L2} \\ v_{g,L3} \end{pmatrix} = l \frac{d}{dt} \begin{pmatrix} i_{LSC,L1} \\ i_{LSC,L2} \\ i_{LSC,L3} \end{pmatrix} + \begin{pmatrix} v_{LSC,L1} \\ v_{LSC,L2} \\ v_{LSC,L3} \end{pmatrix} \quad (1)$$

For the LSC, voltage-oriented control is used. Therefore currents and voltages must be transformed to the grid voltage  $v_g$  oriented reference frame, which is a rotating coordinate system aligned to the rotating grid voltage phasor (denoted here by the superscript  $\angle v_g$ ). By applying Park transformation on (1), the resulting dq components of the chosen rotating reference are as follows:

$$v_{g,d}^{\angle v_g} = l \frac{d i_{LSC,d}^{\angle v_g}}{dt} - \omega_0 l i_{LSC,q}^{\angle v_g} + v_{LSC,d}^{\angle v_g} \quad (2)$$

$$v_{g,q}^{\angle v_g} = l \frac{d i_{LSC,q}^{\angle v_g}}{dt} + \omega_0 l i_{LSC,d}^{\angle v_g} + v_{LSC,q}^{\angle v_g} \quad (3)$$

The transformation angle of the grid voltage  $v_g$  reference frame is defined as:

$$\Theta_g = \int \omega_0 dt = \arctan \left( \frac{v_{g,\beta}^{\angle 0}}{v_{g,\alpha}^{\angle 0}} \right) \quad (4)$$

Where  $\omega_0$  is the synchronous angular speed corresponding to the speed of the rotating reference frame  $\angle v_g$ . According to

Clarke transformation,  $v_{g,\alpha}^{\angle 0}$  and  $v_{g,\beta}^{\angle 0}$  are the phasor components in the fixed coordinate system (denoted by  $\angle 0$ ). Fig. 7 illustrates the complex phasor diagram of the LSC. In grid voltage-oriented rotating reference frame it can be concluded that  $v_{g,q}^{\angle v_g} = 0$ .

The reference voltages of the LSC by adjusting both (2) and (3) will be:

$$v_{LSC,d\_ref}^{\angle v_g} = v_{g,d}^{\angle v_g} - v'_{LSC,d}{}^{\angle v_g} + \omega_0 l i_{LSC,\beta}^{\angle v_g} \quad (5)$$

$$v_{LSC,q\_ref}^{\angle v_g} = v_{g,q}^{\angle v_g} - v'_{LSC,q}{}^{\angle v_g} - \omega_0 l i_{LSC,d}^{\angle v_g} \quad (6)$$

Where:

$$v_{LSC,d}^{\angle v_g} = k_p \left( 1 + \frac{1}{sT} \right) (i_{LSC,d\_ref}^{\angle v_g} - i_{LSC,d}^{\angle v_g}) \quad (7)$$

$$v_{LSC,q}^{\angle v_g} = k_p \left( 1 + \frac{1}{sT} \right) (i_{LSC,q\_ref}^{\angle v_g} - i_{LSC,q}^{\angle v_g}) \quad (8)$$

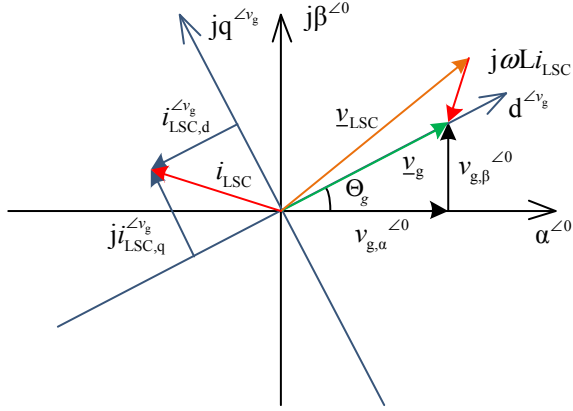


Fig. 7. LSC complex phasor diagram

The active and reactive power of the LSC are expressed as:

$$p_{LSC} = v_{g,d}^{\angle v_g} i_{LSC,d}^{\angle v_g} + v_{g,q}^{\angle v_g} i_{LSC,q}^{\angle v_g} \quad (9)$$

$$q_{LSC} = v_{g,q}^{\angle v_g} i_{LSC,d}^{\angle v_g} - v_{g,d}^{\angle v_g} i_{LSC,q}^{\angle v_g} \quad (10)$$

Since the q-component  $v_{g,q}^{\angle v_g}$  of the LSC in symmetrical case is zero, we can conclude, that the d-component  $i_{LSC,d}^{\angle v_g}$  and the

q-component  $-i_{LSC,q}^{\angle v_g}$  of the LSC are proportional to the active and reactive power respectively. By neglecting converter power losses the power flow between the DC and AC sides can be expressed as:

$$p_{LSC} = v_{DC} i_{DC} \approx v_{g,d}^{\angle v_g} i_{LSC,d}^{\angle v_g} \quad (11)$$

Consequently it can be concluded, that the DC-link voltage is controlled through adjusting the d-component  $i_{LSC,d}^{\angle v_g}$  of the LSC. The reference value for the corresponding d-component current is given by:

$$i_{LSC,d\_ref}^{\angle v_g} = k_p \left( 1 + \frac{1}{sT} \right) (v_{DC\_ref} - v_{DC}) \quad (12)$$

Equations (7), (8) and (12) form the basic control scheme for the LSC. The reactive current characteristic function in Fig. 8 sets the reference value of the q-component  $i_{LSC,q\_ref}^{\angle v_g}$  to support the grid with reactive power during short-time grid faults. This is required in certain grid codes. The LSC has always active current priority in order to preserve the power balance in the dc-link.

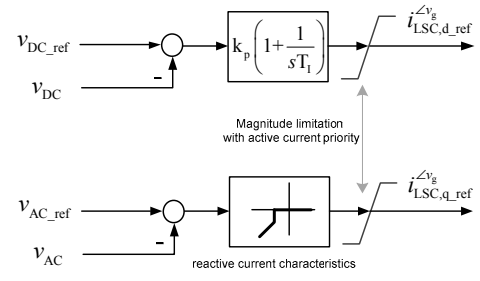


Fig. 8. Structure for generating LSC current reference values

Fig. 9 shows the current controller of LSC. The cross-coupling terms of the voltage across the line inductance and the grid voltage are fed forward so that the PI-controllers only have to provide a fast transition of the current to the respective set-values. The reference voltage values  $v_{LSC,d\_ref}^{\angle v_g}$ ,  $v_{LSC,q\_ref}^{\angle v_g}$  are transformed back to the fixed reference frame and passed from the DSP as reference values for the PWM modules.

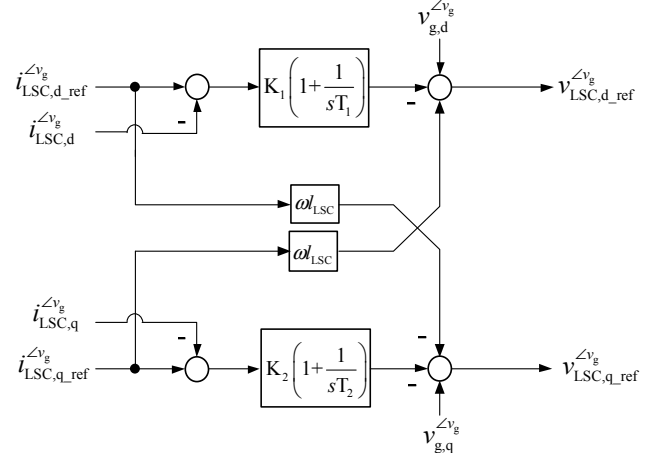


Fig. 9. LSC current control

### B. MSC Control

Independent control of active and reactive power of the generator can be achieved through the MSC. Here likewise voltage-oriented control is used based on stator voltage-oriented reference frame. Flux-oriented control is a common practice in electrical drives. However, power system engineers are more familiar with the terms active and reactive currents instead of electrical torque and excitation current.

The MSC control concept is based mainly on the asynchronous machine equations. The system of equations for the DFIG consists of two voltage equations, two flux equations and an equation of motion which are given by the following:

*Voltage equations:*

$$\underline{v}_S^{\angle} = r_s \underline{i}_S^{\angle} + \frac{d\underline{\psi}_S^{\angle}}{dt} + j\omega_k \underline{\psi}_S^{\angle} \quad (13)$$

$$\underline{v}_R^{\angle} = r_r \underline{i}_R^{\angle} + \frac{d\underline{\psi}_R^{\angle}}{dt} + j(\omega_k - \omega_R) \underline{\psi}_R^{\angle} \quad (14)$$

$\omega_k$  is an arbitrary speed corresponding to the rotating reference frame denoted by an empty superscript  $\angle$ .

Flux linkages:

$$\underline{\psi}_S^\angle = l_S \underline{i}_S^\angle + l_h \underline{i}_R^\angle \quad (15)$$

$$\underline{\psi}_R^\angle = l_h \underline{i}_S^\angle + l_R \underline{i}_R^\angle \quad (16)$$

Equation of motion:

$$\frac{d\omega_R}{dt} = \frac{1}{\theta_m} (\psi_{S,d}^\angle i_{S,q}^\angle - \psi_{S,q}^\angle i_{S,d}^\angle + t_m) \quad (17)$$

The inductances in (15), (16) are defined as:

$$l_S = l_h + l_{\sigma S} \quad (18)$$

$$l_R = l_h + l_{\sigma R} \quad (19)$$

In the steady-state, from (13), (15), and by neglecting the stator resistance, the stator voltage equation can be rewritten as:

$$\underline{v}_S^\angle = j\omega_k (l_S \underline{i}_S^\angle + l_h \underline{i}_R^\angle) \quad (20)$$

Hence the complex phasor of the rotor current is defined as:

$$\underline{i}_R^\angle = -\frac{X_s}{X_h} \underline{i}_S^\angle - j \frac{v_S^\angle}{X_h} \quad (21)$$

In stator voltage oriented coordinates (denoted by  $\angle v_S$ ):

$$\underline{i}_{R,d}^{\angle v_S} = -\frac{X_s}{X_h} \underline{i}_{S,d}^{\angle v_S} \quad (22)$$

$$\underline{i}_{R,q}^{\angle v_S} = -\frac{X_s}{X_h} \underline{i}_{S,q}^{\angle v_S} - \frac{|v_S|}{X_h} \quad (23)$$

The stator active and reactive power equations are given by:

$$p_S = v_{S,d}^{\angle v_S} i_{S,d}^{\angle v_S} + v_{S,q}^{\angle v_S} i_{S,q}^{\angle v_S} \quad (24)$$

$$q_S = v_{S,q}^{\angle v_S} i_{S,d}^{\angle v_S} - v_{S,d}^{\angle v_S} i_{S,q}^{\angle v_S} \quad (25)$$

Assuming that the reference values for stator active and reactive power outputs are known, and by substituting the voltage values in the stator oriented reference frame ( $v_{S,d} = v_S$  and  $v_{S,q} = 0$ ), we get:

$$\underline{i}_{R,d\_ref}^{\angle v_S} = -\frac{p_{S\_ref}}{|v_S|} \frac{X_s}{X_h} \quad (26)$$

$$\underline{i}_{R,q\_ref}^{\angle v_S} = -\frac{q_{S\_ref}}{|v_S|} \frac{X_s}{X_h} - \frac{|v_S|}{X_h} \quad (27)$$

From the rotor voltage in (14) and the stator voltage equation (20) we obtain the following:

$$\underline{v}_R^\angle = r_R \underline{i}_R^\angle + j s \left( x_h \frac{v_S^\angle - j X_h \underline{i}_R^\angle}{j X_s} + X_R \underline{i}_R^\angle \right) \quad (28)$$

In stator voltage oriented coordinates (denoted by  $\angle v_S$ ), rotor voltage can be written in dq components as:

$$v_{R,d}^{\angle v_S} = s \frac{X_h}{X_s} v_{S,d}^{\angle v_S} + r_R i_{R,d}^{\angle v_S} - i_{R,q}^{\angle v_S} s \sigma X_R \quad (29)$$

$$v_{R,q}^{\angle v_S} = r_R i_{R,q}^{\angle v_S} + i_{R,d}^{\angle v_S} s \sigma X_R \quad (30)$$

Here a leakage coefficient  $\sigma = (1 - X_h^2 / X_R X_S)$  is introduced.

Based on PI controllers, the control transfer function for the rotor current controller is give as:

$$v_{R,d}^{\angle v_S} = r_R i_{R,d}^{\angle v_S} = k_p \left( 1 + \frac{1}{sT} \right) (i_{R,d\_ref}^{\angle v_S} - i_{R,d}^{\angle v_S}) \quad (31)$$

$$v_{R,q}^{\angle v_S} = r_R i_{R,q}^{\angle v_S} = k_p \left( 1 + \frac{1}{sT} \right) (i_{R,q\_ref}^{\angle v_S} - i_{R,q}^{\angle v_S}) \quad (32)$$

To be able to pass the outputs of the rotor current controller  $v_{R,d}^{\angle v_S}$  and  $v_{R,q}^{\angle v_S}$  as reference values into the MSC, the signals have to be transformed into the rotor reference frame. This will require the knowledge of the rotor (position) angle  $\Theta_R$ .

$\Theta_R$  could be obtained by measuring the rotor position using a position encoder sensor. Alternatively the rotor transformation angle  $\Theta_R$  and the slip transformation angle are obtained mathematically using the measured stator and rotor currents as follows:

$$\Theta_g = \arctan \left( \frac{i_{R,\beta}^{\angle R}}{i_{R,\alpha}^{\angle R}} \right), \Theta_R = \arctan \left( \frac{i_{R,q}^{\angle v_S}}{i_{R,d}^{\angle v_S}} \right)$$

The coordinate system ( $\alpha^{\angle R}, j\beta^{\angle R}$ ) is a fixed reference frame (stationary) with respect to the rotor. From the definition of the slip speed:  $\omega_{sl} = \omega_0 - \omega_R = \frac{d\Theta_{sl}}{dt}$ , the slip transformation angle is defined as  $\Theta_{sl} = \Theta_g - \Theta_R$ .

The MSC complex phasor diagram in Fig. 10 is based on this sensorless approach.

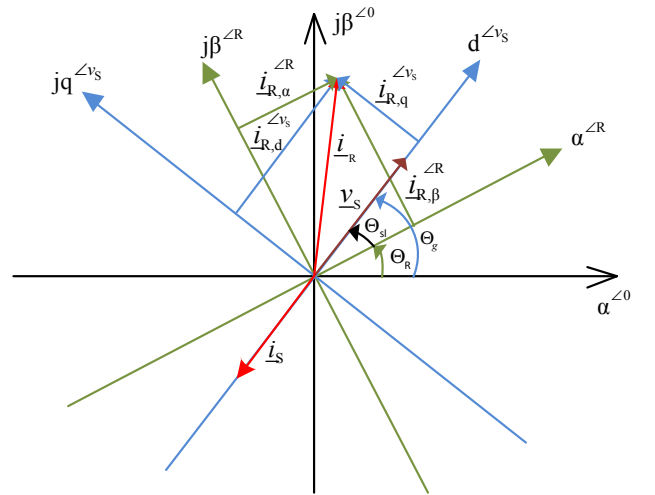


Fig. 10. MSC complex phasor diagram

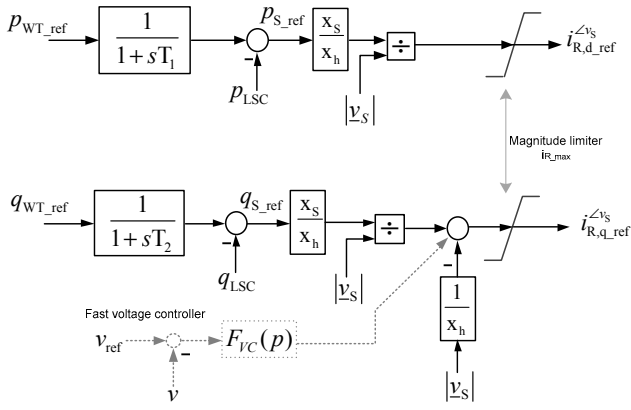


Fig. 11. Structure for generating MSC (rotor) current reference values

MSC control scheme is shown in Fig. 11 and Fig. 12. Input variables are  $p_{WT\_ref}$  and  $q_{WT\_ref}$ , the reference real and reactive power of the wind turbine respectively. To get the stator reference power through, LSC power is subtracted from these values. In real wind turbine operation  $p_{WT\_ref}$  is provided by the speed controller whereas  $q_{WT\_ref}$  can be chosen arbitrarily within certain limits.

In the experimental rig both active and reactive power setpoints can be set arbitrarily from the PC user interface in case of manual speed mode. When switching on the emulator mode the active power reference value is set according to the control technique explained in the next section.

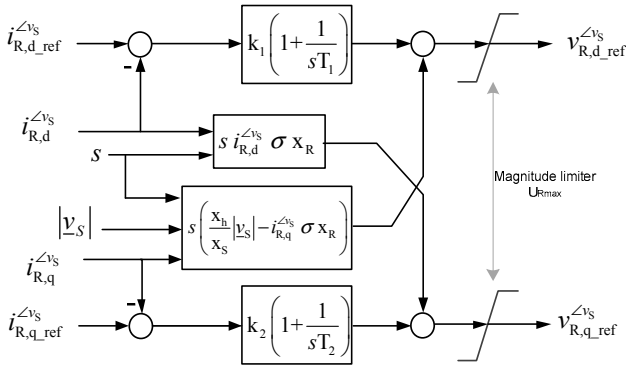


Fig. 12. MSC (rotor) current control

## VI. WIND TURBINE MODELING, CONTROL AND EMULATION

A control model for the wind turbine emulator is implemented in a software environment. The model consists of a wind turbine mechanical model with pitch and speed control. Recorded wind speed data are the input. The model generates the mechanical torque setpoint for the drive and the reference value of active power for the MSC. Depending on the rotor speed, the reference value of the active power is derived using typical power characteristics of a wind turbine.

### A. Wind Turbine Mechanical Model

The mechanical power extracted from the wind can be calculated as:

$$p_m = \frac{1}{2} \rho A_{rot} c_p(\lambda, \beta) v_w^3 \quad (33)$$

Where  $\rho$  is the air density,  $A_{rot}$  is the cross-section through which the air mass is streaming,  $c_p$  is the power coefficient and  $v_w$  is the wind speed. Wind turbine manufacturers give the specific value for a turbine as a function  $c_p$  of the pitch angle  $\beta$  and tip-speed ratio  $\lambda$ . The tip-speed ratio is defined as:

$$\lambda = \omega_r R / v_w \quad (34)$$

Where  $R$  is the radius of rotor blade and  $\omega_r$  is the speed of the turbine. There is a fixed relationship between  $\omega_r$  and  $\omega_g$  given by the gear transmission ratio. The turbine model is based on the steady-state power characteristics of the turbine; the function  $c_p(\lambda, \beta)$  was modeled based on [5].

### B. Pitch and Speed Control

The main task of pitch (rotor blade) control is to limit wind turbine mechanical power (torque) at high wind speeds to the nominal value and to keep the rotor speed inside the desired range. Using a PI controller the speed error is compensated, when the generator speed exceeds the nominal speed (see bottom part of Fig. 14). Usually the chosen nominal speed for the generator is  $1.2\omega_s$  or (1.2 per unit). Fig. 13 shows a typical power curve of a wind turbine.

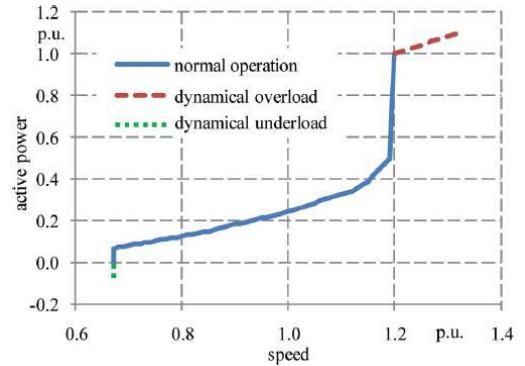


Fig. 13. Typical power curve of a wind turbine [2]

### C. Emulation Technique

Various papers [1], [6] discussed in details different techniques of wind turbine emulation. The technique applied at the experimental rig is based on Fig. 14.

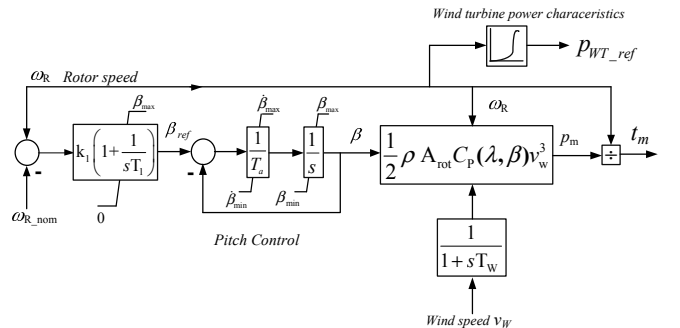


Fig. 14. Speed and pitch control with the power conversion model

In this control structure, the mechanical torque  $t_m$  of the wind turbine model is sent as a setpoint to the driving motor. Simultaneously, the wind turbine reference power  $p_{WT\_ref}$  is generated through the wind turbine speed-power characteristics. The optimum power is stored in a look-up table. When the speed exceeds the nominal speed the pitch controller is activated. Thus the mechanical power of the wind turbine model will be reduced and consequently the shaft speed will therefore decrease. The actual wind turbine emulator control is implemented in LabVIEW. A further paper will discuss in details the theoretical concept, technical implementation and features of the existing emulator.

## VII. USER INTERFACE, COMMISSIONING AND EXPERIMENTAL RESULTS

### A. PC User Interface

The Front Panel of the software LabVIEW is the user interface for operating the experimental rig. The Front Panel consists of three subpanels. Fig. 15 shows the DFIG control subpanel. For educational and illustrative purposes, setpoints for LSC and MSC control are manually adjustable with certain limitations during manual speed control operation. These setpoints are sent to the DSP through a serial interface. During emulator operation, the ‘‘Control Power Curve’’ button is activated and consequently manual adjustments of setpoints are deactivated. Measured and calculated currents, voltages and powers are visualized flexibly on the Front Panel. Fig. 16 shows the FRT testing subpanel. The user can choose the fault type and perform short-circuit tests with adjustable durations.

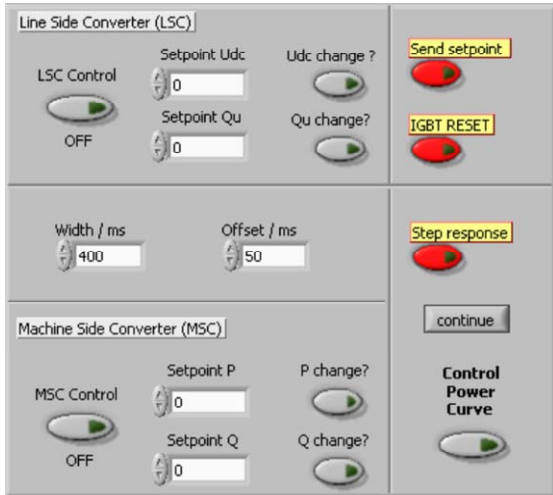


Fig. 15. Main subpanel - DFIG control

### B. Commissioning Procedure of the Experimental Rig

The operation of the experimental rig starts by connecting the rotor side circuit to the grid through the transformer. First, the LSC is connected and the LSC control is activated. The LSC regulates the DC-link voltage to stabilize it at constant level (here approx. 350V). The next step is to start the motor in manual speed control mode to operate at a subsynchronous speed of 1200 rpm. MSC control is afterwards activated; at

this point stator voltage and grid voltage are synchronized. Only then the stator side circuit is connected to the grid. As a result, the DFIG is coupled successfully to the grid.

At this stage, the DFIG can operate in partial load or full load operation depending on the given speed level. The active and reactive power setpoints can be set from the subpanel during manual speed operation. At any point after synchronization and coupling the DFIG to the grid, the emulator control mode can be activated and the DFIG will operate according to the power tracking control algorithms mentioned in the previous section. This is done by pressing the start button in the middle column of Fig. 17 and loading the set of recorded wind speed data.

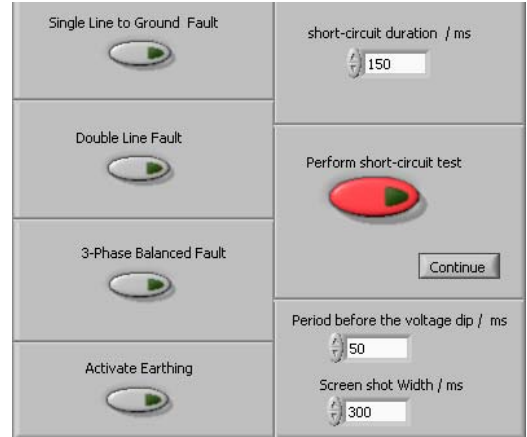


Fig. 16. FRT subpanel

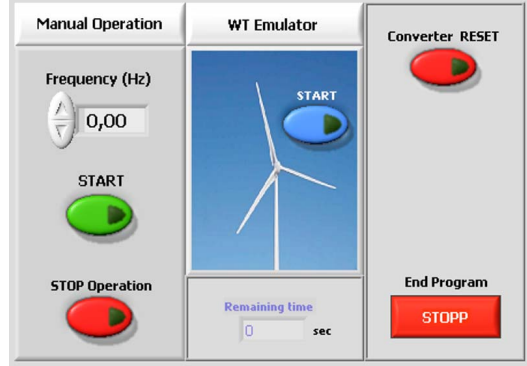


Fig. 17. Motor drive control subpanel

### C. Experimental Results

Fig. 18 demonstrates the results during emulator operation. Recorded data of fluctuating wind speed are processed during a period of 100 s. The base wind speed is set to 12 m/s corresponding to the rotor nominal speed of 1.2 pu. The active power value in per units is referenced to the rated total active power (stator and rotor electrical power). The nominal torque can be calculated as follows:

$$t_{\text{nom(pu)}} = \frac{p_{\text{nom(pu)}}}{\omega_{\text{nom(pu)}}} = \frac{1}{1.2} = 0.833 \text{ pu} \quad (35)$$

Experimental results of FRT capability for the same DFIG system are given in [3].

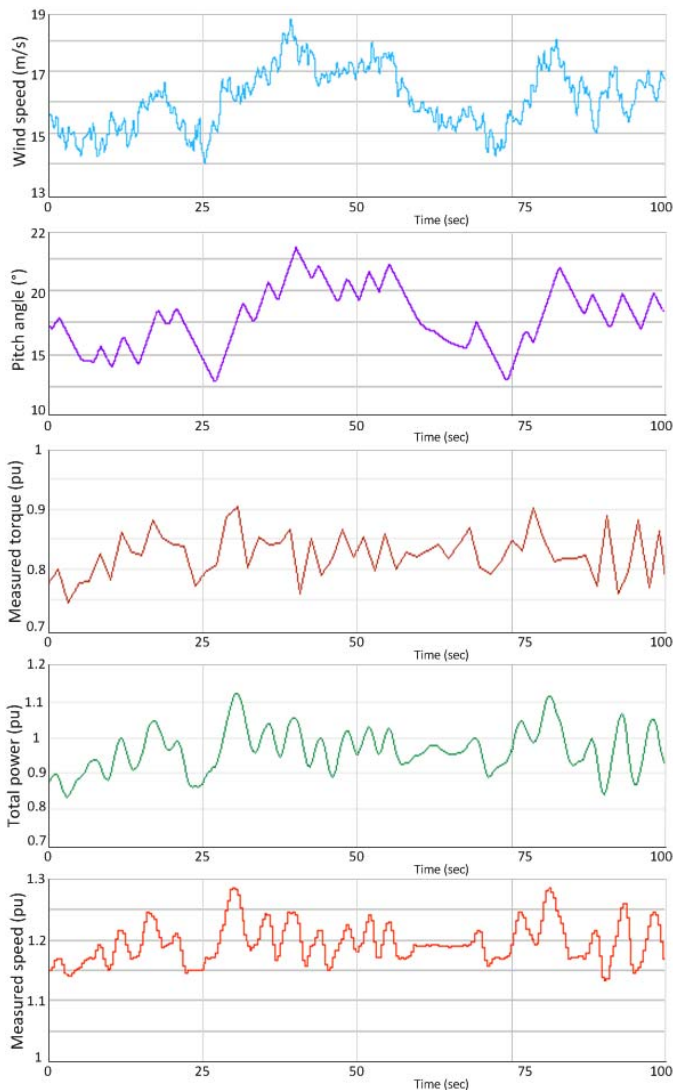


Fig. 18. Behavior of the DFIG system during emulator operation using variable wind speed data input.

### VIII. CONCLUSION

The developed experimental rig focuses on the demonstration of the control and operational principles of a modern DFIG based wind turbine.

The detailed documentation during different implementation phases of the experimental rig offers an open source technical know-how for the students at the university. Based on that experience, the university developed the DFIG control system for a commercial training system of a wind energy generation unit in cooperation with the company Lucas-Nülle. The specifications of the training unit are found on the company website:

(<http://www.lucas-nuelle.com/316/apg/1226/EWG+1+Wind+power+plants.htm>).

### IX. REFERENCES

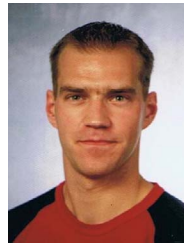
- [1] R. Pena, J. C. Clare, G. M. Asher, "Doubly-fed induction Generator Using Back-to-Back PWM Converters and Its Application to Variable-Speed Wind-Energy Generation", *IEE Proc.-Electr. Power Appl.*, Vol. 143, No. 3, pp. 231-241, 1996.

- [2] S. Engelhardt, I. Erlich, C. Feltes, J. Kretschmann, F. Shewarega, "Reactive Power Capability of Wind Turbines Based on Doubly Fed Induction Generators", *IEEE Transactions on energy conversion*, vol. 26, no. 1, March 2011.
- [3] T. Neumann, C. Feltes, I. Erlich, "Development of an Experimental Rig for Doubly-Fed Induction Generator based Wind Turbine". *Modern Electric Power Systems 2010*, Wroclaw, Poland.
- [4] National Instruments, "LabVIEW User Manual" E2003. Available: [www.ni.com/pdf/manuals/320999e.pdf](http://www.ni.com/pdf/manuals/320999e.pdf)
- [5] S. Heier, "Grid Integration of Wind Energy Conversion Systems", Kassel University, John Wiley & Sons, Germany, 2006, p. (35 – 38).
- [6] R. Cárdenas, R. Peña, Member, "Sensorless Vector Control of Induction Machines for Variable-Speed Wind Energy Applications", *IEEE TRANSACTIONS ON ENERGY CONVERSION*, VOL. 19, NO. 1, MARCH 2004.

### X. BIOGRAPHIES



**Mohammad Suwan** (1985) received his M.Sc. degree in electrical engineering from the University Duisburg Essen, Germany in June 2011. Since August 2011 he is doing his Ph.D. studies in the department of Electrical Power Systems at the same University. His research interests are focused on grid integration of renewable energy and modeling and control of wind turbine converters and solar inverters. He is a member of VDE.



**Tobias Neumann** (1977) received his Dipl.-Ing. degree in electrical engineering from the University Duisburg Essen, Germany in 2009. Since January 2010 he is doing his Ph.D. studies in the Department of Electrical Power Systems at the same University. His research interests are focused on wind energy generation, control and grid integration. He is student member of IEEE.



**Christian Feltes** (1979) received his Dipl.-Ing. degree in electrical engineering from the University Duisburg-Essen, Germany in 2005. From January 2006 to February 2011 he worked in the research staff of the Department of Electrical Power Systems at the same University. Since March 2011 he is working as grid integration engineer in the Offshore Wind Engineering department at RWE Innogy GmbH in Hamburg. His research interests are focused on wind energy generation, control, integration and dynamic interaction with electrical grid.



**Istvan Erlich** (SM'06) was born in 1953. He received his Dipl.-Ing. degree in electrical engineering from the University of Dresden, Germany in 1976. After his studies, he worked in Hungary in the field of electrical distribution networks. From 1979 to 1991, he joined the Department of Electrical Power Systems of the University of Dresden again, where he received his PhD degree in 1983. In the period of 1991 to 1998, he worked with the consulting company EAB in Berlin and the Fraunhofer Institute IITB Dresden respectively. During this time, he also had a teaching assignment at the University of Dresden. Since 1998, he is Professor and head of the Institute of Electrical Power Systems at the University Duisburg-Essen/Germany. His major scientific interest is focused on power system stability and control, modeling and simulation of power system dynamics including intelligent system applications. He is a member of VDE and senior member of IEEE.